Theoretical study of electronic and magnetic properties of MnN

B. R. Sahu and Leonard Kleinman
Department of Physics, University of Texas at Austin, Austin, Texas 78712-0264, USA
(Received 17 March 2003; revised manuscript received 30 June 2003; published 4 September 2003)

We present electronic structure calculations of manganese mononitride (MnN) in its tetragonally distorted NaCl structure using density-functional theory within the generalized gradient approximation. The structure with an antiferromagnetic arrangement of the spins on the Mn ions is found to be the energetically stable phase of the MnN compound. The chemical bonding between Mn and the N ion is of a mixed type (i.e., mainly ionic but partly metallic and covalent). The calculated spin magnetic moment on the Mn ion is close to the experimental value of $3.3\mu_B$.

DOI: 10.1103/PhysRevB.68.113101 PACS number(s): 71.20.Be, 71.15.Dx

The study of the interaction between the $3d$ shell of transition metals and the valence s and p shell of light elements such as O, N, and C has been one of the active areas of research for last few decades. Among the binary compounds so formed, the transition metal mononitrides have been extensively studied in last few years in order to understand their electronic and magnetic properties. Extensive calculations of the three earliest members of the $3d$, $4d$, and $5d$ series transition-metal nitrides were performed by Stampfl *et al.*[1] There are a few theoretical works on the structural stability of early transition-metal mononitrides. Noteworthy among these works[2–5] are calculations with the wrong crystal and magnetic structure of manganese nitride (MnN). Most of the confusion was due to the absence of experimental data on the low-temperature crystal and magnetic structure of MnN. Janotti *et al.*,[5] to gain insight into Mn doped GaN, studied zinc-blende MnN. Recently, Suzuki *et al.*[6] synthesized single-phase MnN without any interstitial nitrogen defects. They used combined x-ray and neutron-diffraction techniques to determine the crystal and magnetic structure of MnN. In this paper, we perform electronic structure calculations of single-phase MnN using the full-potential linear augmented plane-wave (FLAPW) method[7] and generalized gradient approximation (GGA).[8] To the best of our knowledge, this is the first theoretical work on MnN with the correct crystal and magnetic structure.

The previous theoretical studies on MnN focussed on predicting the crystal and magnetic structure using arguments based on total energy differences and densities of states. Eck *et al.*,[2] used the tight-binding linear muffin-tin orbital (TB-LMTO) method within the atomic sphere approximation (ASA) and predicted the stable phase of MnN to be a nonmagnetic zinc-blende structure. Häglund *et al.*[3] using the LMTO-ASA method found it to be a ferromagnetic NaCl structure with magnetic moment of $3.03\mu_B$ on Mn and $0.14\mu_B$ on the N atom. Using the FLAPW method a ferromagnetic NaCl structure with the spin magnetic moment of $2.18\mu_B$ on Mn atom was predicted by Shimizu *et al.*[4] Surprisingly, antiferromagnetism and the possibility of distortion was not considered in any of these theoretical studies.

The crystal structure determined by Suzuki *et al.*[6] is a tetragonally distorted NaCl structure with the lattice parameters $a=8.042$ bohrs, $c=7.916$ bohrs, and $c/a=0.984$. The magnetic structure is the first kind of antiferromagnetic (AFM) ordering, i.e., the magnetic moments of the Mn atoms align ferromagnetically in a c plane and the ferromagnetic (FM) c planes couple antiferromagnetically with each other ($T_N=650$ K). Each Mn atom is surrounded by six N atoms arranged in a slightly distorted octahedral cage. The tetragonally distorted NaCl structure used in Ref. 6 is face-centered tetragonal (fct) which can equally well be regarded as a body-centered tetragonal (bct) structure with $a(\text{bct})=a(\text{fct})/\sqrt{2}$ and $c(\text{bct})=c(\text{fct})$.

We have used the bct structure with 4 atoms per unit cell (2 Mn and 2 N atoms) for our calculations. The calculations are performed using the FLAPW method[7] and a spin-polarized GGA (Ref. 8) within the framework of density-functional theory.[9,10] The basis set inside each nonoverlapping muffin-tin sphere is split into core and valance subsets. For Mn, $1s$, $2s$, and $2p$ and for N only $1s$ orbitals are in the core subset. Sphere radii of 2.1 (1.8) bohrs were used for Mn (N) initially. The valence part is treated with the potential expanded into spherical harmonics up to $l=6$. The valence wave functions inside the spheres are expanded up to $l=10$. In all cases we use an APW+local orbital[11,12] type basis with additional local orbitals for Mn $3s$ and $3p$ semicore states. The calculations were tested for accuracy with respect to the **k**-point sampling and for the plane-wave expansion parameter $R_{mt}K_{max}$ where K_{max} is the plane-wave cutoff and R_{mt} is the smallest of all muffin-tin spheres in the structure under consideration. $R_{mt}K_{max}=8$ and 105 **k** points in the irreducible wedge of the bct Brillouin Zone (BZ) turns out to be sufficient for the accuracy of the results reported in this paper (0.1 mRy for the total energy per cell and 0.001 Bohr magnetons for the magnetic moment).

The equilibrium volume was determined by energy versus volume optimization at the experimental c/a ratio and c/a optimization at this equilibrium volume gives the optimized lattice parameters a and c. Because the calculated c/a ratio is nearly identical to the experimental one, it was not necessary to reoptimize the volume at the calculated c/a ratio. The optimized values are displayed in Table I. Note that the calculated ferromagnetic c/a ratio is very nearly $\sqrt{2}$, i.e., the crystal would have the rock salt structure except for a very small magnetostriction. The lattice constants are too small by 1.6%, typical of local-density approximation or GGA calculations, relative to the experimental value of Suzuki *et al.*[6]

TABLE I. The magnetization (in Bohr magnetons) and cohesive energy per MnN moiety (in eV) calculated at the experimental and optimized lattice constants (in bohrs) for antiferromagnetic and ferromagnetic MnN. We use a body-centered tetragonal unit cell. For the distorted simple cubic cell multiply a by $\sqrt{2}$. The antiferromagnetic magnetization is calculated within Mn spheres of radius $0.4703c/2$ and $0.5c/2$ (in parenthesis). The ferromagnetic magnetic moment is per Mn atom.

	a	c	c/a	M_s	E_{coh}
AF(opt)	5.586	7.804	1.397	2.94(3.01)	9.562
AF(expt)	5.686	7.916	1.392	3.08(3.15)	9.483
Experiment[a]	5.686	7.916	1.392	3.30	
FM(opt)	5.529	7.799	1.411	3.06	9.470
FM(expt)	5.686	7.916	1.392	3.22	9.378

[a]Reference 6.

The cohesive energy (defined to be the total ground-state energy of the compound minus the sum of total atomic ground-state energies of the spin-polarized constituents) of the AFM phase is about 92 meV per MnN unit larger than that of the FM phase (see Table I). The spin-polarized atomic ground-state energies are calculated in a 30-Å supercell and at the Γ point in the BZ. The atomic energies are Mn $=-2317.0281$ Ry and N$=-103.1305$ Ry. This shows that the tetragonally distorted NaCl structure with the antiferromagnetic spin ordering on Mn ions along the c direction is indeed the ground-state stable phase of MnN (at least with respect to the ferromagnetic and undistorted NaCl structures) in conformity with the experimental findings of Suzuki *et al.*[6]

Figures 1 and 2 show, respectively, the l-projected spin density of states (DOS) for the N and one of the two identical (except for a reversal of their spins) Mn atoms. The projections are within spheres whose radii are $0.4703c/2$ and $0.5297c/2$ for Mn and N, respectively. The reason for this choice, related to the position of the minimum of the charge density along the c axis , will be explained later. The exchange splitting between the peaks in the DOS of the up- and down-spin d states is 3.16 eV. In Table I, we list the AFM spin magnetic moment within the Mn spheres and, in the FM phase, the spin moment is listed per unit cell. Our calculations of the spin magnetic moment on the Mn ion in the AFM phase are close to the experimental value of $3.3\mu_B$ (see Table I). We got the spin magnetic moment of $3.08\mu_B$ on the Mn ion with the experimental lattice constants and $2.94\mu_B$ with the calculated lattice constants using a $0.4703c/2$ sphere radius in each case. Using a $c/4$ sphere radius we obtained even better agreement with experiment (see Table I).

Figure 3 displays the valence charge density along the c axis in the optimized lattice constant case. Our original choice of muffin-tin spheres was very far from the relative size of the Mn and N ions as seen in Figs. 3 and 4. Therefore, although it made very little difference in the final result (it lowered the cohesive energy by ~ 0.1 mRy) we chose spheres which touched at the c-axis charge density minimum and repeated the calculation . This was continued until the input and output c-axis minima agreed. We find the rather small charge density of 71 millielectrons/bohr^3 at a point 47.03% of the way from Mn to N is the minimum. There are 4.462 electrons within the Mn sphere and 5.363 within the N. Dividing the remaining 2.175 interstitial electrons equally between the two atoms, results in 6.451 N electrons and 5.549 Mn electrons, i.e., the Mn (N) has an ionic charge of $+$ ($-$) 1.45 e. Except in those cases where the charge density essentially vanishes between the atoms, the ionicity of a crystal cannot be given a precise value. To obtain some idea of the uncertainty in the ionicity we repeated the calculation using two equal spheres of radius $c/4$. We obtained 4.762 electrons within the Mn sphere and 5.035 within the N sphere. After sharing the remaining 2.204 electrons equally

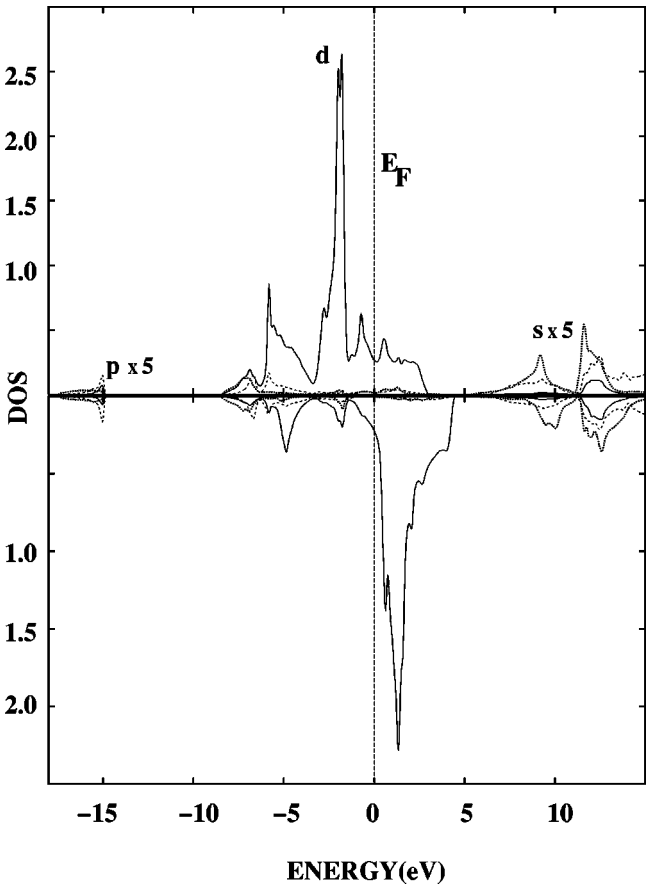

FIG. 1. The majority and minority spin—s (dotted lines), p (dashed lines), and d (solid lines)—projections of the DOS (electrons per cell per eV) for a Mn sphere of radius $0.4703c/2$ in the tetragonally distorted antiferromagnetic NaCl structure.

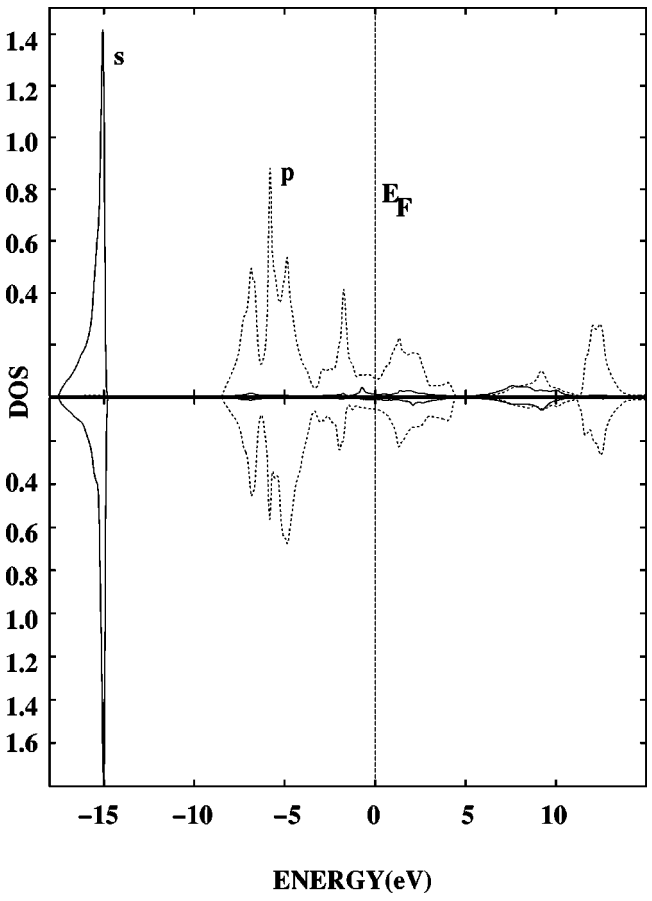

FIG. 2. The majority and minority spin—*s* (solid lines) and *p* (dashed lines)—projections of the DOS (electrons per cell per eV) for a N sphere of radius 0.5297*c*/2.

between the two atoms, we obtained an ionicity of 1.14 electrons. We note in (Table I) that the cohesive energy is 9.562 eV. This may be compared with the 7.23 eV of NaCl.

In addition to the ionic bonding there is some bonding due to the Mn *d* orbitals overlapping the N *p* orbitals and a much

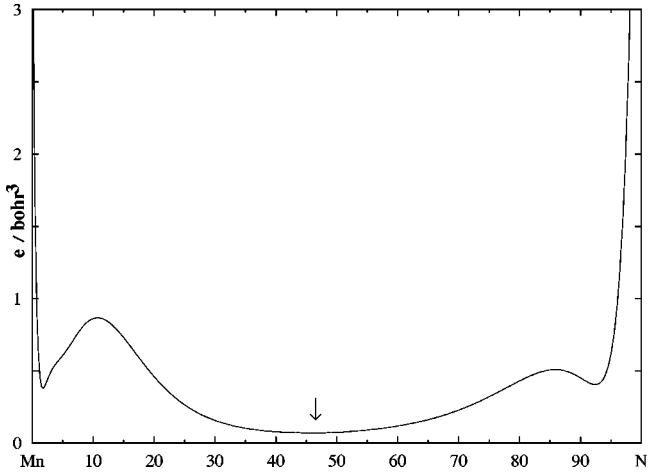

FIG. 3. Valence electron charge density (for optimized lattice constants) as a percentage of the distance along the *c* axis from Mn to N. The arrow points to the minimum charge density of 0.0708 electrons per cubic bohr.

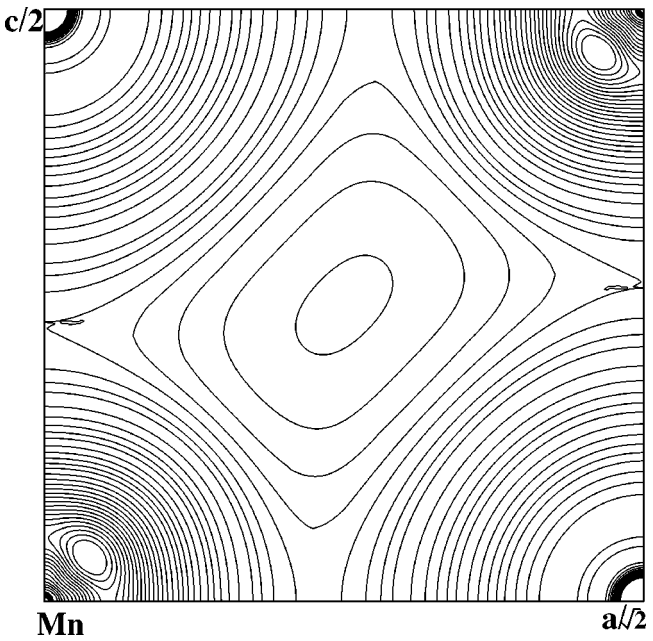

FIG. 4. Valence electron charge-density contour plot from Mn to its N neighbors at $c/2$ and $a/\sqrt{2}$ in units of millielectrons per cubic bohr. The central contour has a value of 31. The contours increase in steps of 10 to 101 then in steps of 20 to 201, in steps of 30 to 451, and between 451 and 1001 in steps of 50. Contours above 1001 are not shown.

smaller amount due to the *d*-*s* overlap. The d_{xz}, d_{yz}, and $d_{x^2-y^2}$ orbitals point away from the N atoms and do not contribute but $d_{3z^2-r^2}$ overlaps p_z and d_{xy} overlaps p_{x+y} and p_{x-y} (remember our unit cell is rotated by 45° relative to that in Ref. 6). Looking at the majority spin *d* DOS in Fig. 1, the very small piece at -15 eV comes from *s*-*d* hybridization. The somewhat larger piece at 13 eV may represent transverse N *p* orbitals inside the Mn sphere which would have xz, yz, and x^2-y^2 symmetry about the Mn site. The largest peak comes mainly from the three nonbonding orbitals. Because the *p* functions are odd and the *d* functions are even, at the center of BZ the integrated overlap of the d_{xy} and $d_{3z^2-r^2}$ Bloch functions with the nitrogen *p* Bloch functions vanishes and therefore they also contribute a small amount to the nonbonding peak. The structure on either side of the main peak represents bonding and antibonding combinations of the overlapping functions from the outer parts of the BZ. Since some of the antibonding states are pushed above E_F, the *p*-*d* overlap results in some covalent bonding. This can also be seen in Table II where the majority spin d_{xz} and $d_{x^2-y^2}$ partial charges within the Mn sphere are all about

TABLE II. The up- and down-spin *d*-orbital content in the Mn sphere of radius 0.4703*c*/2 for the antiferromagnetic optimized case.

	d_{xy}	$d_{yz}=d_{xz}$	$d_{x^2-y^2}$	$d_{3z^2-r^2}$
Mn↑	0.594	0.815	0.835	0.578
Mn↓	0.184	0.097	0.149	0.186

0.82 while those of $d_{3z^2-r^2}$ and d_{xy} are around 0.58, due to the fact that some of their projected DOS is pushed above E_F. On the other hand, the DOS at the Fermi surface is quite finite so that the interstitial electrons may also be said to have a metallic component. The picture is perhaps clarified by the valence charge-density contour plot of Fig. 4. One sees that most of the charge lie within the inscribed spheres (actually 82% of the charge within 51.64% of the unit-cell volume), which tends to weakly bond along the *c* axis and somewhat more weakly along the *a* axis but that the charge density looks weakly metallic in the middle of the face.

In conclusion, we have shown using the FLAPW method and the GGA that the tetragonally distorted antiferromagnetic NaCl structure, deduced from x-ray and neutron-diffraction studies, is the stable phase of MnN. The bonding is shown to be highly ionic but of a mixed type. The bonding states are formed between *p* orbitals of N and $d_{3z^2-r^2}$ and d_{xy} orbitals of Mn , the antibonding combination of which provide almost all the density of states at the Fermi energy and therefore the metallicity of MnN. The nonbonding *d* states are mainly d_{yz}, d_{xz}, and $d_{x^2-y^2}$ orbitals and contribute the major part of the magnetic moment of the Mn atom.

This work was supported by the Welch Foundation (Houston, TX), the NSF under Grant No. DMR-0073546 and Texas Advanced Computing Center (TACC), University of Texas at Austin.

[1] C. Stampfl, W. Mannstadt, R. Asahi, and A.J. Freeman, Phys. Rev. B **63**, 155106 (2001).
[2] B. Eck, R. Dronskowski, M. Takahashi, and S. Kikkawa, J. Mater. Chem. **9**, 1527 (1999).
[3] J. Häglund, G. Grimvall, T. Jarlborg, and A.F. Guillermet, Phys. Rev. B **43**, 14 400 (1991).
[4] H. Shimizu, M. Shirai, and N. Suzuki, J. Phys. Soc. Jpn. **66**, 3147 (1997).
[5] A. Janotti, Su-Huai Wie, and L. Bellaiche, Appl. Phys. Lett. **82**, 766 (2003).
[6] K. Suzuki, Y. Yamaguchi, T. Kaneko, H. Yoshida, Y. Obi, H. Fujimori, and H. Morita, J. Phys. Soc. Jpn. **70**, 1084 (2001).
[7] P. Blaha, K. Schwarz, G. K. H. Madsen, D. Kvasnicka, and J. Luitz, computer code WIEN2K, Vienna University of Technology, Vienna, Austria, 2001.
[8] J.P. Perdew, K. Burke, and M. Ernzerhof, Phys. Rev. Lett. **77**, 3865 (1996).
[9] P. Hohenberg and W. Kohn, Phys. Rev. **136**, B864 (1964).
[10] W. Kohn and L.J. Sham, Phys. Rev. **140**, A1133 (1965).
[11] E. Sjöstedt, L. Nordström, and D.J. Singh, Solid State Commun. **114**, 15 (2000).
[12] G.K.H. Madsen, P. Blaha, K. Schwarz, E. Sjöstedt, and L. Nordström, Phys. Rev. B **64**, 195134 (2001).